2021-11-30

X-Ray Polarimetry with the Daksha Space Telescope

B.Tech Project I

Parth Sastry

Advisor **Prof. Varun Bhalerao**

Email parth.sastry@iitb.ac.in

Abstract X-ray astronomy has come a long way since its beginnings via detectors launched on the nose cones of sounding rockets back in the 1950s. X-ray polarimetry, on the other hand, is a largely unexplored area within this otherwise mature field. With the launch of Astrosat in 2015, we have been able to obtain sensitive measurements of X-ray polarization data via the CZTI instrument onboard. With the upcoming launch of IIT-B's own *Daksha* Space Telescope, we seek to create a software pipeline in Python, to perform polarization analysis with the data to be obtained from the planned 17 onboard Cadmium Zinc Telluride (CZT) detectors. Daksha's high sensitivity and large field of view will make it the workhorse for high energy transient discovery and characterisation in the coming decade. The end goal of the project is to perform extensive polarimetric sensitivity calculations with the software pipeline so developed, to be able to gauge the capabilities of *Daksha* and its Minimum Detectable Polarization for various sources.

Contents

1 Introduction

Polarization of photons is a fundamental property reflecting their nature as electromagnetic waves. A photon represents a 'packet' of electric and magnetic fields oriented perpendicular to the direction of motion, owing to which light is classified as a transverse wave. These electric and magnetic fields evolve in time according to Maxwell's equations.

Polarization describes the configuration of the electric field, by convention. The magnetic field is interrelated with the same.

All light is polarized, but different photons from a source may have different polarizations. If the distribution of polarization angles is uniform, the source radiation is said to have zero net polarization. If not, it has some net polarization. In astrophysics, generation of non-zero net polarizations requires a net deviation from spherical symmetry in either the physical structure of the source, or the magnetic field configuration of the system [1].

X-ray astronomy deals with the detection and study of X-ray radiation (~ 100keV ~ 100eV) from astronomical objects. Earth's atmosphere is opaque to X-rays [2], and hence X-ray detectors have to be taken above the earth's atmosphere to make observations. X-ray observatories are typically aboard orbiting satellites to allow for long-term measurement, but early measurements were taken with instruments on-board weather balloons.

Polarization measurements of X-ray radiation from astrophysical sources contain a wealth of information about the emission mechanism behind this radiation, as well as the orientation and geometry of the structure itself. This is of particular interest to us when studying Gamma Ray Bursts (GRBs), which are highly energetic flashes of radiation primarily in the X-ray and gamma ray spectrum. The emission mechanism of Gamma Ray Bursts remains little understood [3] and polarization measurements of GRBs and GRB afterglows may provide insights into how these electromagnetic events occur. This is discussed further in Section 4.

Daksha is a proposed high-energy transients mission comprising of two satellites monitoring the entire sky in the $1-1000$ keV range. The primary goals of *Daksha* are to study the electromagnetic counterparts of gravitational waves, and prompt emission Gamma Ray Bursts. This project is an effort to create a software pipeline in Python to perform polarization analysis using data to be gathered from *Daksha* in the future. It is primarily influenced by a similar pipeline created to perform

polarization analysis on data gathered from Astrosat-CZTI, which is the hard X-ray detector aboard India's first astronomical satellite Astrosat [4] [5].

Section 2 talks about the theory behind how X-ray polarimetry is performed and how it's done in the case of pixellated semiconductor detectors like the Cadmium Zinc Telluride detectors aboard Astrosat and Daksha. Section 3 is a short overview of the major processing blocks that have been coded in my current Python pipeline and the other processing blocks that have been taken from elsewhere. It also talks a bit about why we've been working on coding a new pipeline when a previous pipeline already exists for Astrosat-CZTI. Section 4 shows a comparison of results obtained via my current processing pipeline for a particular GRB, compared to data obtained from the previous pipeline. Section 5 concludes the report and mentions what the next steps and processing blocks left to code are.

2 An Overview of X-Ray Polarimetry

2.1 Theory

Available X-ray instrumentation is able to measure the intensity of X-rays (the number of photons per unit time), the energies of X-rays (via conversion of that energy to charge or heat), and the positions of X-rays or, more precisely, the positions at which an X-ray deposits charge via interactions. Since X-ray polarization cannot be measured directly, the X-rays must first undergo some interaction that converts the polarization information to a directly measurable quantity, typically intensity or position [6].

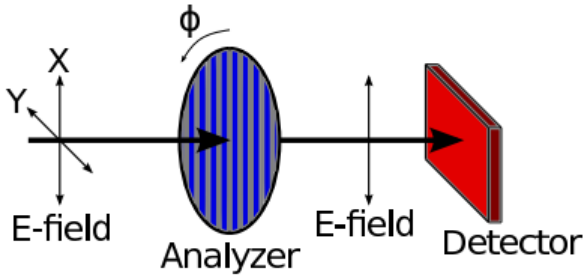

Figure 1: *Polarization Analyzer : A linear polarization analyzer is rotated and the associated detector records the intensity of photons (counts) at each angle as a modulation curve. Image Credits: [1]*

Consider a rotating polarization analyzer shown in Figure 1. As the analyzer is rotated, the intensity of photons detected changes. The resulting histogram of counts versus rotation angle is called the Modulation Curve, which in general has the form -

$$S(\phi) = A + B\cos^2(\phi - \phi_0) \tag{1}$$

here, ϕ_0 is the polarization angle at which maximum intensity is recorded. The modulation amplitude is $a = (S_{\max} - S_{\min})/(S_{\max} + S_{\min}) = B/(A + 2B)$. Given a modulation curve, we can obtain ϕ_0 via fitting.

The modulation factor μ_{100} is the modulation amplitude as measured for a 100% polarized beam. In an ideal world, this value would be 1, but in real-life

we'd detect some radiation even perpendicular to the polarization angle (hence, S_{min} won't be 0). For a polarimeter with some μ_{100}, a background count rate R_{bkg} independent of rotation angle, the polarization fraction of a source with modulation amplitude a and count rate R_{src} is -

$$P = \frac{a}{\mu_{100}} \frac{R_{\text{src}} + R_{\text{bkg}}}{R_{\text{src}}} \tag{2}$$

In designing an X-ray polarimeter, it is essential that the system (analyzer/detector and telescope) can reach sufficient statistical accuracy for the measurements required. The traditional figure of merit is the 'Minimum Detectable Polarization' (MDP) [7]. The polarization fraction, P, is a non-negative quantity. Any particular measurement of P will produce a value greater than 0. The MDP is the largest fluctuation expected to occur with a probability of 0.01.

Equivalently, the MDP is the smallest polarization that can be detected at a 99% confidence level. The MDP for an observation of duration T is -

$$\text{MDP} = \frac{4.29}{R_{\text{src}}\mu_{100}} \sqrt{\frac{R_{\text{src}} + R_{\text{bkg}}}{T}} \tag{3}$$

Usually, a scientifically useful polarization measurement entails determination of both P and ϕ_0. This is a joint measurement of two parameters and requires additional statistics beyond those suggested by the MDP [8], however we don't go into those in this report or project.

The method of obtaining the previously described modulation curve changes depending on the polarimeter and the physical processes used for polarization measurement. The principle behind polarimetry using the Cadmium Zinc Telluride Detectors used in Astrosat and Daksha is that of Compton scattering of high-energy photons with electrons present within the detector. Polarimeters based on this principle are called Compton polarimeters.

2.1.1 Compton Polarimeter

At energies above a few tens of keV, Compton scattering is the dominant interaction of X-rays with matter. When the X-ray energy is an appreciable fraction of the rest mass energy of an electron, the electron will recoil during the interaction, taking energy from the photon. The basic working of any Compton Polarimeter is shown in Figure 2.

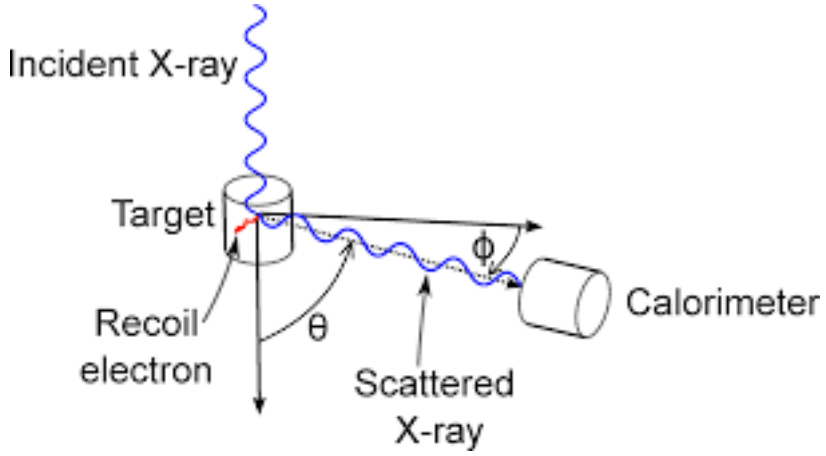

Figure 2: *Working Principle behind any Compton Polarimeter. Image Credits: [1]*

The cross-section of scattering is given by the Klein-Nishina formula -

$$\frac{d\sigma_C}{d\Omega} = \frac{r_e^2}{2}\left(\frac{E'}{E}\right)^2\left[\frac{E'}{E} + \frac{E}{E'} - 2\sin^2\theta\cos^2\phi\right] \tag{4}$$

where r_e is the classical electron radius, E is the initial photon energy, E' is the final photon energy, and we have averaged over the polarization of the final photon [9]. ϕ is measured with respect to the incident polarization angle ϕ_0. For scattering angles near 90°, the azimuthal distribution of the scattered photon is strongly dependent on the X-ray polarization, making Compton scattering an effective tool for polarization analysis. The dependence of $\frac{d\sigma_C}{d\Omega}$ on ϕ is shown in Figure 3.

2.2 Semiconductor X-Ray Detectors

Semiconductor detectors have developed rapidly in recent years and are now used in a variety of fields, including X-ray and Gamma ray astronomy, nuclear physics and nuclear medicine. In comparison with gas detectors and scintillators, they have good energy resolution and can form much more compact systems.

The typical operation of semiconductor detectors is based on collection of the charges, created by photon interactions, through the application of an external electric field. The choice of the proper semiconductor material for a radiation

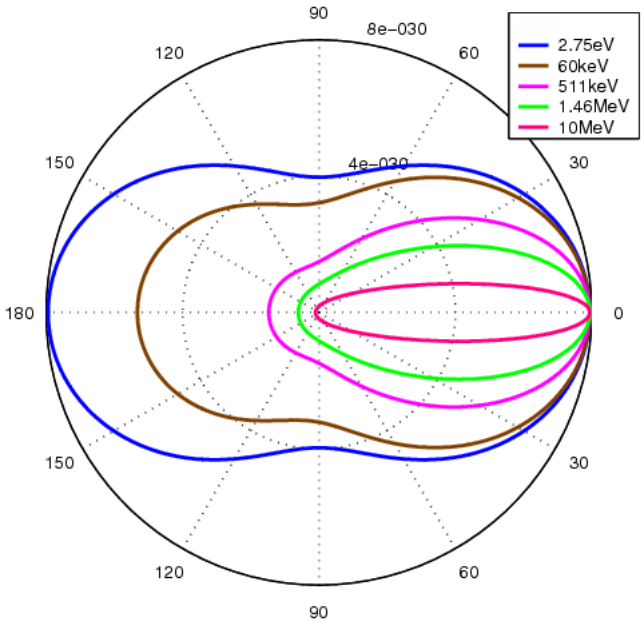

Figure 3: *The Klein-Nishina cross section as a function of energy, plotted on a polar plot. The angle here is ϕ. Image Credits : User Dscraggs on Wikipedia*

detector is mainly influenced by the energy range of interest. There are three primary interactions of X-rays and Gamma rays with matter that are important when considering X-ray measurements. -

1. **photoelectric absorption** : the interacting photon transfers all its energy to an atomic electron
2. **compton process** : the interacting photon transfers only a fraction of its energy to an outer electron, producing a hot electron and a degraded photon
3. **pair production** : interacting photon with energy above a threshold energy interacts within the Coulomb field of the nucleus producing an electron and positron pair

Consider a simple planar detector - a slab of a semiconductor material with metal electrodes on the opposite faces of the semiconductor - Figure 4. Photon interactions produce electron-hole pairs in the semiconductor volume through

the discussed interactions. The interaction is a two-step process where the electrons created in the photoelectric or Compton process lose their energy through electron-hole ionization.

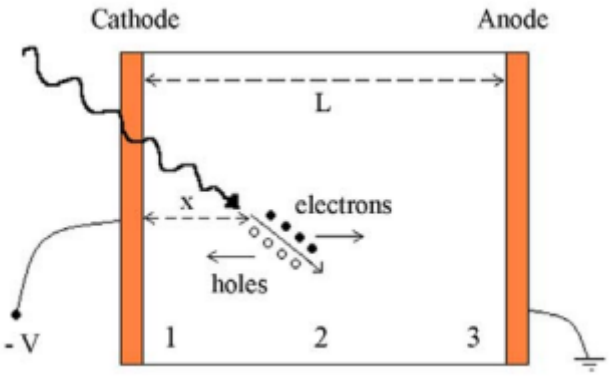

Figure 4: *Planar Configuration of a semiconductor detector. Electron-hole pairs generated are swept away to the appropriate electrode via an external electric field. Image Credits : [10]*

The number of electron-hole pairs generated is proportional to the photon energy. If E is the incident photon energy, the number of electron-hole pairs generated is -

$$N = \frac{E}{w}$$

here, w is the average electron-hole pair production energy. The generated charge Q is thus $Q = Ne = Ee/w$ [10]. Measurement of this generated charge at the anode (anode, because electrons move much faster than the corresponding holes, allowing us to take readings faster) allows us to calculate the incident energy E of the photon. Arranging multiple detectors in a tiled configuration allows us to create an ensemble pixellated detector.

The detectors used in Daksha and Astrosat are Cadmium Zinc Telluride (CdZnTe, or CZT) detectors, where the semiconductor material used is $Cd_{1-x}Zn_xTe$.

2.3 Compton Polarimetry with Pixellated Detectors

Compton polarimetry with pixellated detectors works with similar ideas in mind as standard Compton polarimetry discussed in 2.1.1. The major difference in the

case of pixellated detectors, of course, is that we do not have scattering counts for continuously varying ϕ values. The incident photon transfers a fraction of its energy to the recoil electron, which is detected at the anode of the semiconductor detector at the site of incidence (*incident pixel*). A larger part of the photon's energy is transmitted to the scattered photon, which is detected within the detector in some other pixel (*scattered pixel*).

2.3.1 Compton Scattering Events

To try and arrive at an angular distribution of scattering, we treat scattering events occuring in specific pixels as occuring in discrete angular bins, and generate a modulation curve based off of that. This is shown in Figure 5. There are a couple of points to note here -

1. the detection of the Compton scattered photon is expected to occur at the same time as the detection of the incident photon since photon travel time is negligible. This gives us the definition of a **double event** as detection events occurring within the duration of the resolution window of the internal detector clock
2. the Compton scattered photon isn't expected to travel far from the scattering site before getting absorbed, so we only consider double events occurring within **adjacent pixels** to avoid the chance coincidence events that are going to occur (two independent photons arriving within the detector resolution window at different pixels)
3. despite imposing the neighboring pixel criteria, you still observe some chance coincidence events, and thus we impose a third criteria comparing the energies of the two events. This is the **Compton criteria**

For a true Compton scattering event, energy of the scattered photon is always greater than the recoil electron energy for incident photon energies < 280 keV. For lower energy of the incident photons and scattering angles around 90°, the ratio of the energy of the scattered photon and the recoil electron is ≥ 2. This is the Compton criteria, helping us to further weed out chance coincidence events from true scattering events.

So, to summarize - double events occurring in adjacent pixels (Figure 5) that satisfy the Compton Criteria are valid Compton events. Depending on which adjacent pixel the scattering occurred in, we assign this Compton event an **angular bin** ranging from 0° to 360° in increments of 45°. This gives us the observed angular distribution of Compton events that are seen in our data. There

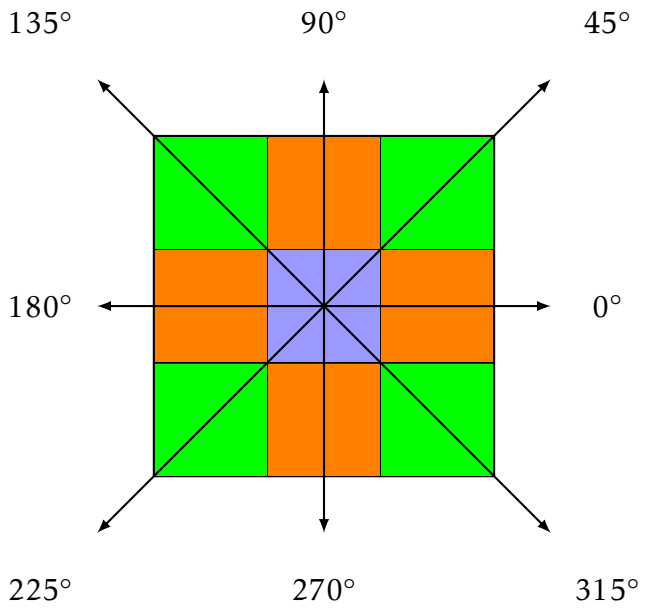

Figure 5: *Central pixel in purple and neighboring pixels. Simultaneous events in these neighboring pixels constitute a valid double event*

are corrections to be made to this distribution, which are discussed in Subsection 2.5

All these results are taken from the PhD thesis of Dr. Tanmoy Chattopadhyay [11] who was responsible for coming up with this pipeline to perform X-ray polarimetry with CZT detectors. Dr Chattopadhyay also coded the pipeline to perform this analysis using the CZT detectors aboard Astrosat, which the current Daksha pipeline is expected to build upon.

2.4 Astrosat and Daksha

Before we move on to discussing what the Astrosat mass model is, why is it required and how does it relate to the Daksha mission, we discuss the two satellites to see what the instruments obtaining our data are, and what payloads do we use for our polarization studies.

2.4.1 Astrosat

Astrosat is a multi-wavelength astronomy mission launched on September 28, 2015. A schematic of the satellite is shown in 6. It is India's first space observatory and has 5 astronomy payloads -

1. twin 38-cm **Ultraviolet Imaging Telescopes (UVIT)** covering Far-UV to optical bands
2. three units of **Large Area Xenon Proportional Counters (LAXPC)** covering medium energy X-rays from 3 to 80 keV
3. a **Soft X-ray Telescope (SXT)** covering the energy range 0.3-8 keV
4. a **Cadmium-Zinc-Telluride coded-mask imager (CZTI)**, covering hard X-rays from 10 to 150 keV
5. a **Scanning Sky Monitor (SSM)** that is placed on a rotating platform to scan the available sky once every six hours in order to locate transient X-ray sources

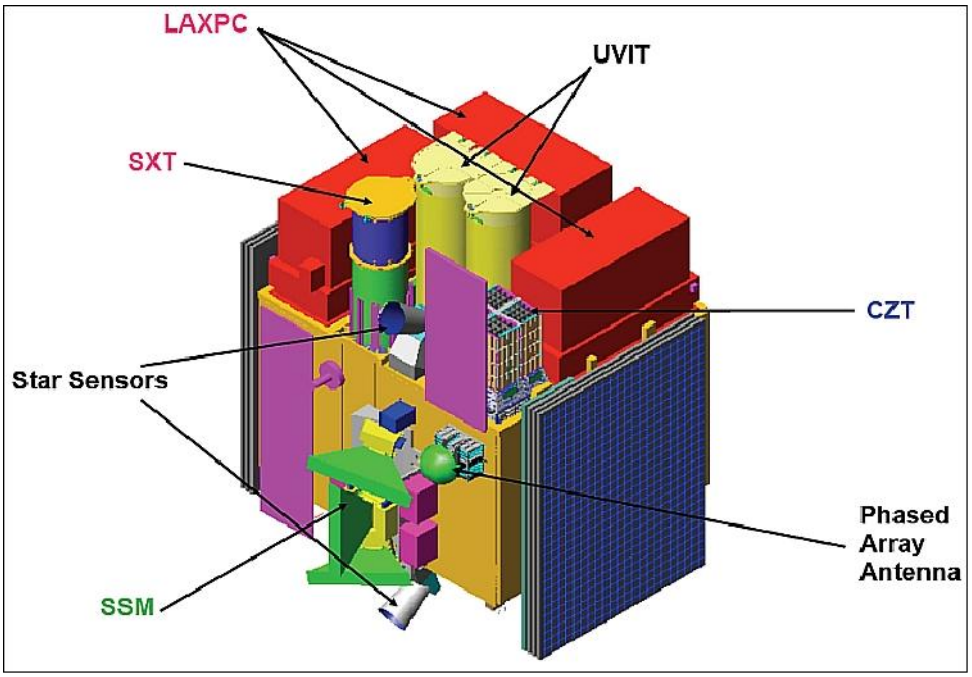

Figure 6: *Illustration of the AstroSat spacecraft and its instrument complement. Image Credit: ISRO*

The CZTI is of primary interest to us, since it covers the hard X-ray energy range

where GRBs (Gamma Ray Bursts) and other transient sources are detected. As stated in the Introduction, an IDL (Interactive Data Language) pipeline already exists to perform polarization analysis using CZTI data.

As validation of our pipeline for Daksha, we made sure to be able to perform polarization analysis of transient sources detected using CZTI via our pipeline, allowing us to compare results and make sure the finished software could still be used while Daksha is in development, on CZTI data.

2.4.2 Daksha

Daksha is a proposed space telescope being developed by IIT-Bombay for detecting high energy counterparts to gravitational wave sources. It will be an order of magnitude more sensitive than any existing mission. It will cover the energy range from 1 keV to ≥ 1 MeV, reaching a sensitivity higher than the *Neil Gehrels Swift Observatory*. Two satellites orbiting on opposite sides of Earth will ensure continuous coverage of the entire sky. [1]

Daksha will have 17 CZT detectors onboard, compared to Astrosat-CZTI's 4 CZT detectors, which will allow us to perform polarization analysis on detected X-ray transients. With more detectors, and a mission comprised of two satellites, Daksha is expected to have higher sky coverage than Astrosat. With its CZT detectors being in different orientations, it is not only expected to detect more transients than Astrosat, but also to help in quantifying any systematic errors in transient polarisation measurements, an advantage over the coplanar quadrants of Astrosat-CZTI.

2.5 The Mass Model

Heading back to performing X-ray polarimetry, we left off at our seemingly complete methodology to obtain the angular distribution of Compton scattering events in our 8 angular bins. The idea behind classifying Compton events and obtaining the angular distribution of the same is sound, but we ignored two glaring problems which we discuss here.

[1] https://www.star-iitb.in/research/daksha

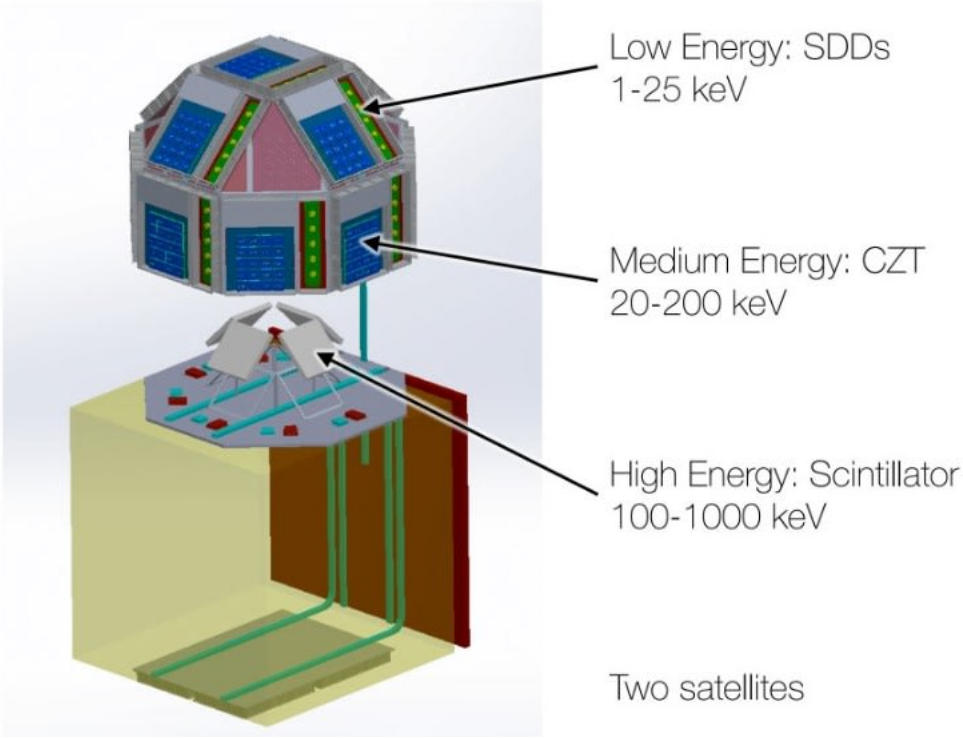

Figure 7: *Proposed design of Daksha. Image Credit: Varun Bhalerao, Santosh Vadawale and the Daksha team*

2.5.1 The necessity of a mass model

The angular bins we assign to each neighboring pixel to compute our angular distribution, however, are unequal. It is readily apparent that the edge pixels (colored orange in Figure 5) occupy a larger angular size than the corner pixels (colored green in Figure 5). This will skew the observed angular distribution drastically in favor of the 0°, 90°, 180° and 270° bins, while reducing the counts in the other bins.

There's another problem. Looking at equation 4 again, we see that we've treated the histogram of scattering events in our detector plane as being the angular distribution in the ϕ plane. This is only true for on-axis osbervations, where $\theta = 90°$. When the event being observed is off-axis, the angular distribution is further complicated, because of the break in symmetry in the pixel geometry with respect to the incident photon direction. The observed distribution will be some form of projection of Figure 3 onto the detector plane.

However, both these effects can be taken care of by normalizing the azimuthal

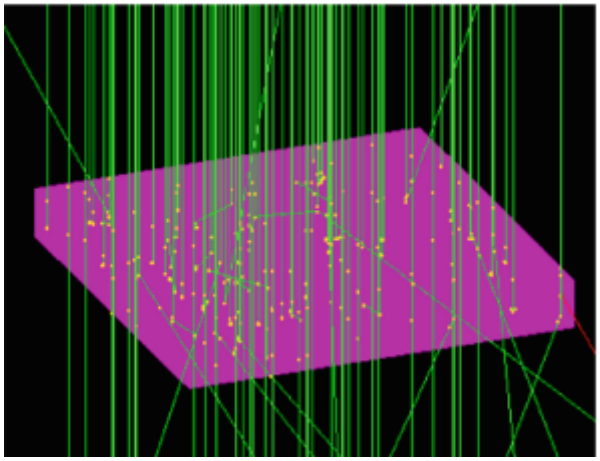

Figure 8: *Simulated diagram for a CZT module (40 mm × 40 mm × 5mm). The module is shined uniformly by X-ray photons shown in green. Image Credits: Tanmoy Chattopadhyay [11]*

distribution by that for 100% unpolarized radiation, of the same spectrum and incident at the same off-axis angle as the source. Thus the observed modulation pattern has to be normalized using the similar modulation pattern for an unpolarized beam. This unpolarized beam is simulated via what are known as mass model simulations. [12]

2.5.2 What is the Mass Model?

The mass model is something that was developed for Astrosat to perform simulations of the passage of radiation through the satellite, and to simulate light-matter interactions within the same. This is done with the help of the GEANT4 toolkit for particle, photons and matter interactions [2]. The mass model is a reproduction (with accurate chemical and geometrical properties) of the Astrosat satellite, within GEANT4 [13].

Individual photons in incoming radiation can then be tracked and simulated as they travel through the satellite and are detected within the detectors. This allows us to simulate the interaction of incoming radiation with the satellite, to yield the final energies (spectrum) and positions (DPH) of photons incident on the detector [14].

The full implementation of how the mass model is implemented for Astrosat

[2]https://geant4.web.cern.ch/

is detailed in reference [14]. The Astrosat mass model allows us to simulate what would happen if we placed some EM source at a specific orientation to the satellite. It's a complex simulation which involves individually tracking the interaction of millions of photons with the particles of the satellite, allowing us to look at what the angular distribution of Compton events (according to our filtering criterion) would look like if the simulated source was of same spectrum and incident at the same off-axis angle as the detected source.

2.5.3 The Daksha Mass Model

The Daksha team has been working on a mass model for Daksha, which will be used for sensitivity calculations, localization, spectroscopic analysis and polarimetric measurements and simulations. The Daksha mass model will give us the angular distribution for an unpolarized beam with the same spectrum and incident at the same off-axis angle as the detected source.

Once we have the modulation pattern for an unpolarized beam, we can perform the required corrections to account for the unequal angular bins and the complications arising from off-axis incidence.

2.5.4 Obtaining the Modulation Curve

If P_i is the count of polarized photons in the i^{th} angular bin, U_i is the count of simulated unpolarized photons in the i^{th} angular bin and $\overline{U}$ is the average number of photons for the unpolarized distribution -

$$C_i = \frac{P_i}{U_i}\overline{U} \tag{5}$$

where C_i refers to the 'corrected' count of polarized photons in the i^{th} angular bin. The distribution of C_i with the angle of the i^{th} angular bin is the modulation curve for our observed data [12]. From the modulation curve, we can obtain the parameters we seek - ϕ_0 and P, the polarization fraction via different possible methods. Two methods are discussed in Section 5.

3 Data Processing Pipeline

A schematic detailing the polarization analysis pipeline is shown below

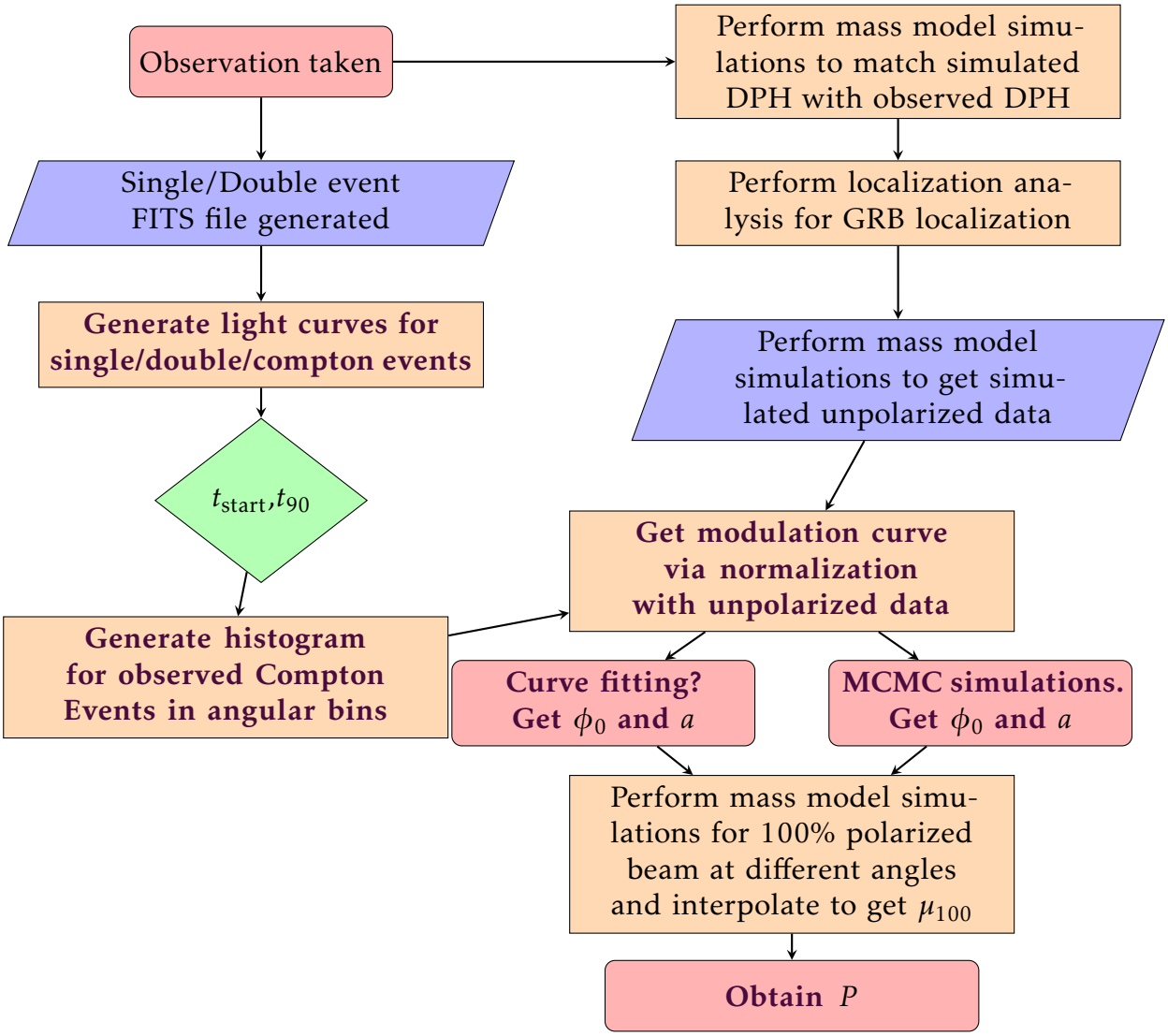

Figure 9: *Bolded steps are those recreated (or to be recreated) in the Python pipeline I am working on*

As stated earlier, there exists an IDL pipeline to perform each of the tasks mentioned in this flowchart. The choice of language is a consequence of when

Astrosat was being planned, when IDL was the preferred language of the astronomy community, and support for open source languages like Python wasn't as prevalent, particularly for astronomical data analysis.

With the advent of Python packages like `astropy` and the general shift of the astronomy community towards open-source and freely available software, unlike IDL which is proprietary, the decision was made to write this pipeline for Daksha (or at least, some parts of it) in Python. That is the goal of this project. We go over the steps being recreated once -

1. **Generate light curves for single/double/compton events** - data arrives in the forms of processed FITS files into this pipeline. Single event files are used to generate a histogram (or light curve) of single event counts during the duration of the GRB. Likewise for double event files, which are processed to find *valid double events* as occurring in adjacent pixels, and *valid compton events*, those of which fulfill the Compton criteria. The histograms (light curves) of these are plotted and saved

2. $\mathbf{t_{start}}$, $\mathbf{t_{90}}$ - t_{start} or the trigger time refers to the start time of the GRB. This is something that can be selected by the user based on the light curve observed. t_{90} is the point of time before which 90% of the total incident photons have been detected. This is something that can be auto-computed by the pipeline, or can be tweaked by the user.

3. **Generate histogram for observed Compton Events in angular bins** - once we have found valid Compton events among the observed double events, we generate our observed angular distribution according to the process detailed in subsection 2.3.1

4. **Get modulation curve via normalization with unpolarized data** - after extensive mass model simulations to find the location of the GRB, we simulate the modulation curve observed for 100% unpolarized data from the same direction and of the same spectrum. We then generate our final, corrected modulation curve according to what we saw in subsection 2.5

5. **Get ϕ_0 and a** - This is the next step of our development which I am currently working on. We need to obtain the parameters of the modulation curve according to one of the two methods specified in reference [14]. Methods detailed in Section 5.

6. **Obtain P** - refer back to Equation 2. To compute P, we need to know μ_{100} - the modulation factor for the 100% polarized beam at the same ϕ_0 as computed in the previous step. This is done via simulating μ_{100} values at some grid of possible ϕ_0 values previously, and then interpolating them to

our computed/fitted ϕ_0

As of this stage, the current pipeline is able to get a modulation curve via normalization with the output of the Astrosat mass model. The results that the current pipeline generates for a sample GRB we chose (GRB 160325A) almost match exactly to what the old pipeline generated. Following this, determining the fitting parameters is the immediate next step, followed by interpolating the mass model simulation outputs for 100% polarized beams to obtain the μ_{100} for our obtained polarization angle ϕ_0 and finally computing the polarization fraction P, the end goal of our polarization analysis.

4 Current Implementation and Results

4.1 Measuring GRB Polarization

4.1.1 What are GRBs?

We have discussed GRBs fleetingly before as the X-ray transient sources we are hoping to study with Daksha. GRBs or Gamma Ray Bursts are immensely energetic explosions observed in distant galaxies. The identification of the progenitors of these explosions is challenging and an object of current study.

As of recent years, LIGO has been detecting gravitational waves via mergers of neutron stars and black holes in far-away galaxies. Finding the electromagnetic counterparts to these gravitational wave sources, which are thought to be GRBs in the case of binary neutron star mergers, would provide us with a wealth of information on the processes that happen during these mergers and their mechanisms of radiation.

Detecting GRBs and analysing the spectrum of their radiation is important, and this project serves to code part of a pipeline which would allow future users of *Daksha* data to analyse and make new insights into these awesome objects.

4.1.2 Are GRBs polarized?

Depends.

Radiation from GRBs is expected to be from outflows moving towards us with relativistic speeds. The emission mechanism behind prompt emission is little understood and there exist various theories for the same. In some mechanisms for emission, polarization is expected to be high and in other cases, it's supposed to be dependent on the geometric viewing angle. Toma et al. (2009) [15] have shown that the statistical distribution of GRB polarization may lift the degeneracy of these theoretical models. Thus, analysing GRB polarization might help us solve the mystery of the way these explosions occur.

4.2 Comparison with Astrosat-CZTI results

4.2.1 GRB160325A

The first GRB I tested my pipeline on, and in fact, the GRB I used to test/debug my pipeline over the course of its development was GRB160325A. A comparison of the various curves involved in analysing a GRB, generated via the two pipelines is given below on new pages, so the comparisons can be seen better.

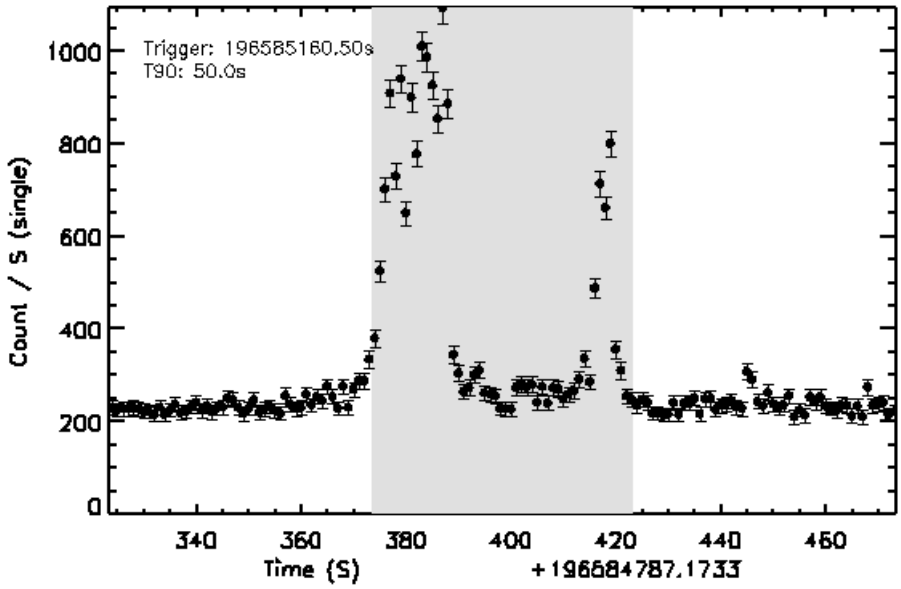

Figure 10: *Single event histogram obtained via the IDL pipeline*

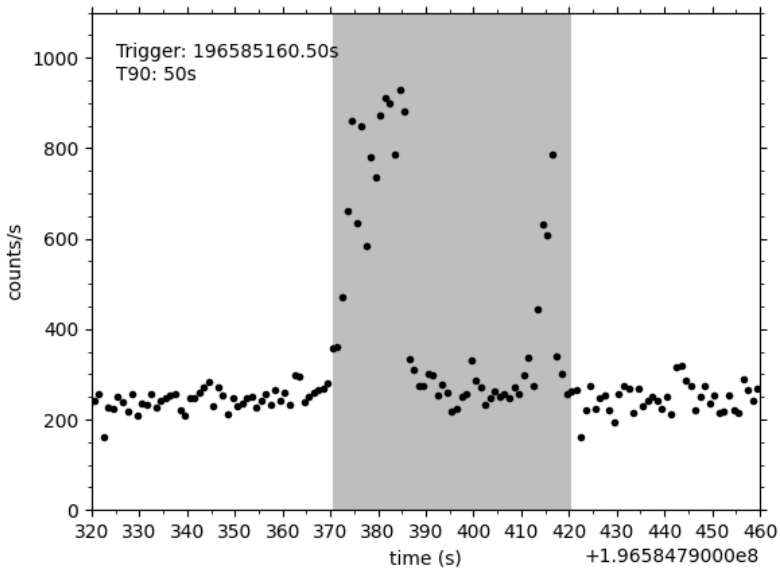

Figure 11: *Single event histogram obtained via the Python pipeline*

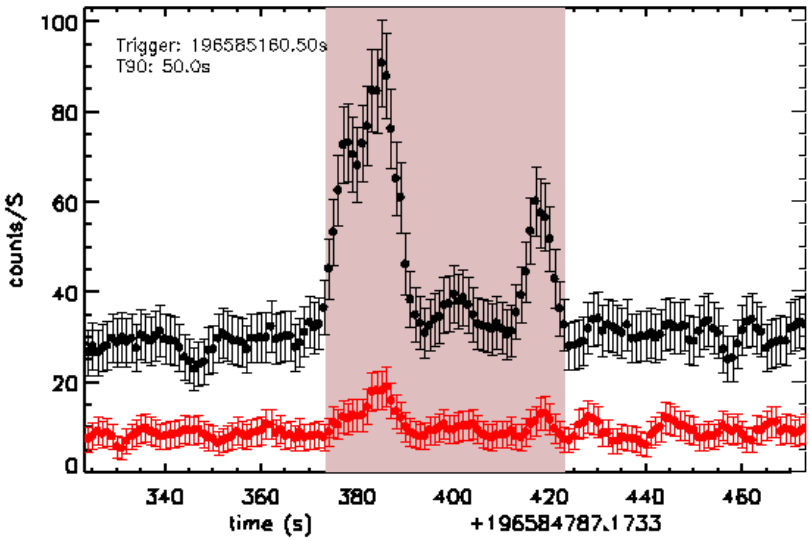

Figure 12: *Compton event histogram obtained via the IDL pipeline. The black curve is a histogram of Compton events, the red curve corresponds to double events that didn't satisfy the Compton criteria*

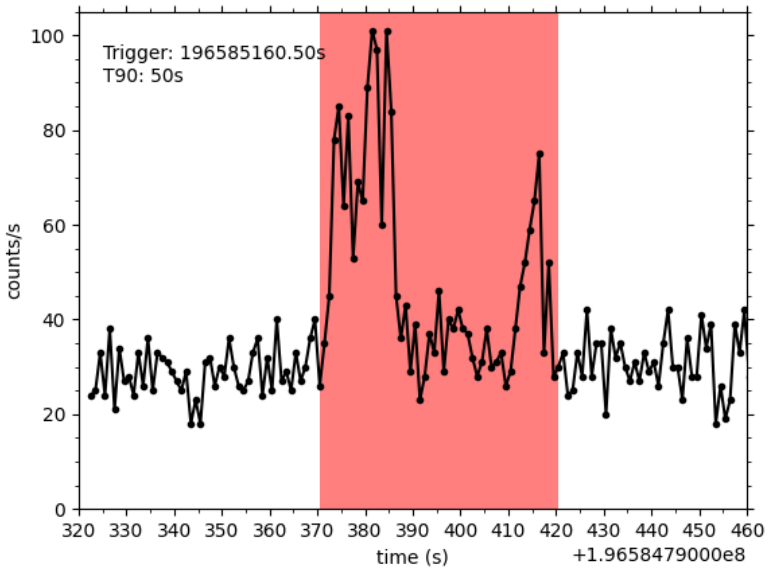

Figure 13: *Compton event histogram obtained via the Python pipeline*

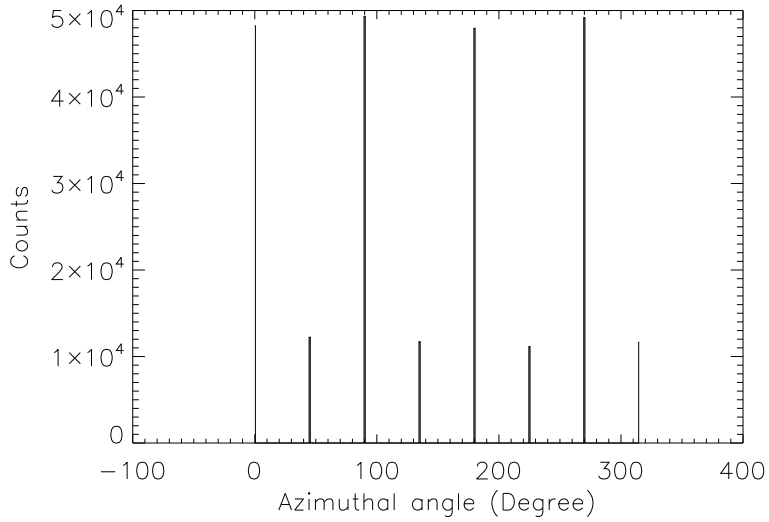

Figure 14: *Angular distribution of the mass model simulations of the unpolarized radiation with same energy spectrum and location obtained via the IDL pipeline*

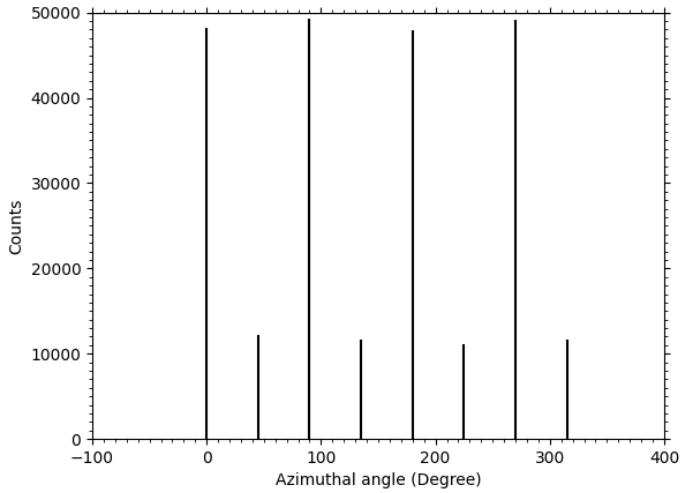

Figure 15: *Angular distribution of the mass model simulations of the unpolarized radiation with same energy spectrum and location obtained via the Python pipeline*

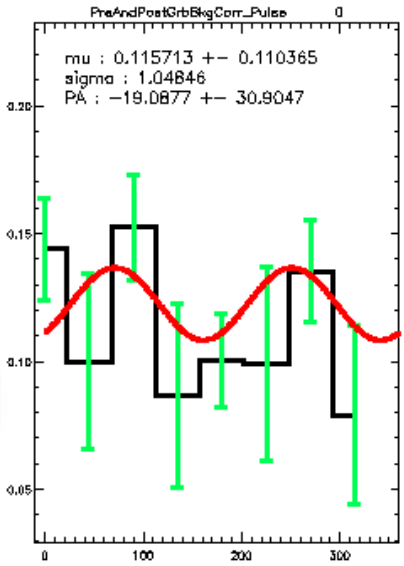

Figure 16: *Modulation Curve after Pre-and-Post background correction obtained via the IDL pipeline*

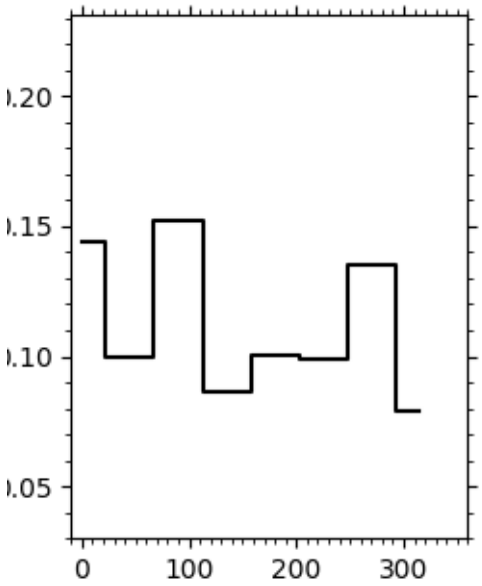

Figure 17: *Modulation Curve after Pre-and-Post background correction obtained via the Python pipeline. Obtaining the errorbars and sinusoidal curve fitting hasn't been done yet.*

5 Next Steps and Conclusion

5.1 Determining Fitting Parameters

We have our corrected modulation curve via our current pipeline in Figure 17, which matches well with the curve obtained via the old IDL pipeline, shown in Figure 16 as we have seen in the previous section. The next step, as seen in the flowchart shown in Figure 9 is to obtain the fitting parameters for this modulation curve via either of two methods - curve fitting, or MCMC simulations

5.1.1 Curve Fitting

We can use standard χ^2 fitting algorithms to fit the modulation curve with a cosine function to estimate the modulation amplitude and the polarization angle, given by -

$$C(\phi) = A\cos(2(\phi - \phi_0 + \pi/2)) + B \tag{6}$$

A,B and ϕ_0 are the fitting parameters. The modulation factor, which is directly proportional to the polarization of the photons, is given by the ratio of A to B, and the polarization angle in the detector plane is given by ϕ_0.

5.1.2 MCMC Simulations

In this case the modulation amplitude, the polarization angle, and their uncertainties are estimated using an Markov-Chain Monte Carlo [16] method based on the Metropolis–Hastings algorithm [17] [18]. The reason for following the approach of Bayesian statistics is the clarity in the fitting procedure and the robustness in the estimation of the parameter uncertainties compared to a χ^2 analysis, particularly for GRBs registering relatively fewer Compton events. [12].

We perform MCMC simulations for a large number (1 million) of iterations. For each iteration, the likelihood is estimated based on randomly sampled parameter

values in Equation 6. A set of parameter values for a given iteration is accepted or rejected by comparing the posterior probability for that iteration with that from the previous iteration (ratio of posterior probabilities should be greater than unity for accepting the parameter values) [12].

Choosing which method to use for finding the fitting parameters for our modulation curve is the next task of coding the polarization pipeline.

5.2 Finding the Polarization Fraction P

$$P = \frac{a}{\mu_{100}} \frac{R_{\text{src}} + R_{\text{bkg}}}{R_{\text{src}}} \tag{7}$$

While P is directly proportional to modulation amplitude a, it is proportional by a factor μ_{100} which depends on the polarization angle ϕ_0. To find μ_{100}, we shall simulate the Mass Model in Geant4 with a large number of fully polarized photons for the same off-axis angle and photon energy distribution of the GRB. To find μ_{100} for our ϕ_0, we interpolate from a table of μ_{100} values computed using Geant4 for a discrete grid of polarization angles.

5.3 MDP calculations for Daksha

$$\text{MDP} = \frac{4.29}{R_{\text{src}}\mu_{100}} \sqrt{\frac{R_{\text{src}} + R_{\text{bkg}}}{T}} \tag{8}$$

The last thing to do is to perform polarimetric sensitivity calculations for Daksha, to estimate what the MDP might be for different source strengths and angles, to get an idea of what the detection capabilities of Daksha might be like when it is fully operational.

All these 'next steps' in Subsections 5.1, 5.2 and 5.3 are ongoing and I expect these to take up the next stage of my B.Tech Project as well, in the next semester.

5.4 Conclusion and Acknowledgements

Huge thanks to all my teammates on the Daksha team - in particular Dr. Suman Bala, Dr. Sourav Palit, Soumya Gupta and Divita Saraogi. They've been super

helpful in handling my relative inexperience in this field, and have always been ready to clear any doubts I may have had.

Dr. Suman Bala and Dr. Sourav Palit have been my direct guides ever since I took up this project, and have been, and will be instrumental to a successful Daksha mission. Thanks immensely as well, to my project advisor Prof. Varun Bhalerao, who's been leading and guiding the entire Daksha team every step of the way. I hope we'll do good work in the second part of this B.Tech Project as well, and I shall be able to make a tiny contribution to this exciting space mission!

References

[1] Philip Kaaret. *X-Ray Polarimetry*. 2016. arXiv: 1408.5899 [astro-ph.IM].

[2] ESO. *Transparency of the atmosphere*. 2010. URL: https://www.eso.org/public/images/atm_opacity/ (visited on 25/11/2021).

[3] Boris E. Stern and Juri Poutanen. 'Gamma-ray bursts from synchrotron self-Compton emission'. In: *Monthly Notices of the Royal Astronomical Society* 352.3 (Aug. 2004), L35–L39. ISSN: 0035-8711. DOI: 10.1111/j.1365-2966.2004.08163.x. URL: http://dx.doi.org/10.1111/j.1365-2966.2004.08163.x.

[4] S. V. Vadawale et al. 'Hard X-ray polarimetry with Astrosat-CZTI'. In: *Astronomy & Astrophysics* 578 (June 2015), A73. DOI: 10.1051/0004-6361/201525686. URL: https://doi.org/10.1051/0004-6361/201525686.

[5] V. Bhalerao et al. 'The Cadmium Zinc Telluride Imager on AstroSat'. In: *Journal of Astrophysics and Astronomy* 38.2 (June 2017). DOI: 10.1007/s12036-017-9447-8. URL: https://doi.org/10.1007/s12036-017-9447-8.

[6] Robert Novick. 'Stellar And Solar X-Ray Polarimetry'. In: *Optical Engineering* 20.1 (Feb. 1981). DOI: 10.1117/12.7972658. URL: https://doi.org/10.1117/12.7972658.

[7] R. Novick et al. 'Polarization of Cosmic X-Ray Sources'. In: *Annals of the New York Academy of Sciences* 302 (1977).

[8] Martin C. Weisskopf, Ronald F. Elsner and Stephen L. O'Dell. 'On understanding the figures of merit for detection and measurement of x-ray polarization'. In: *Space Telescopes and Instrumentation 2010: Ultraviolet to Gamma Ray* (July 2010). DOI: 10.1117/12.857357. URL: http://dx.doi.org/10.1117/12.857357.

[9] F. Lei, A. J. Dean and G. L. Hills. In: *Space Science Reviews* 82.3/4 (1997), pp. 309–388. DOI: 10.1023/a:1005027107614. URL: https://doi.org/10.1023/a:1005027107614.

[10] Stefano Del Sordo et al. 'Progress in the Development of CdTe and CdZnTe Semiconductor Radiation Detectors for Astrophysical and Medical Applications'. In: *Sensors* 9.5 (May 2009), pp. 3491–3526. DOI: 10.3390/s90503491. URL: https://doi.org/10.3390/s90503491.

[11] Tanmoy Chattopadhyay. 'Observational Aspects of Hard X-ray Polarimetry'. In: (2016). DOI: 10.5281/ZENODO.50640. URL: https://zenodo.org/record/50640.

[12] Tanmoy Chattopadhyay et al. 'Prompt Emission Polarimetry of Gamma-Ray Bursts with the AstroSat CZT Imager'. In: *The Astrophysical Journal* 884.2 (Oct. 2019), p. 123. DOI: 10.3847/1538-4357/ab40b7. URL: https://doi.org/10.3847/1538-4357/ab40b7.

[13] S. Agostinelli et al. 'Geant4—a simulation toolkit'. In: *Nuclear Instruments and Methods in Physics Research Section A: Accelerators, Spectrometers, Detectors and Associated Equipment* 506.3 (July 2003), pp. 250–303. DOI: 10.1016/s0168-9002(03)01368-8. URL: https://doi.org/10.1016/s0168-9002(03)01368-8.

[14] Sujay Mate et al. 'The AstroSat mass model: Imaging and flux studies of off-axis sources with CZTI'. In: *Journal of Astrophysics and Astronomy* 42.2 (Aug. 2021). ISSN: 0973-7758. DOI: 10.1007/s12036-021-09763-x. URL: http://dx.doi.org/10.1007/s12036-021-09763-x.

[15] Kenji Toma et al. 'STATISTICAL PROPERTIES OF GAMMA-RAY BURST POLARIZATION'. In: *The Astrophysical Journal* 698.2 (May 2009), pp. 1042–1053. DOI: 10.1088/0004-637x/698/2/1042. URL: https://doi.org/10.1088/0004-637x/698/2/1042.

[16] C.J Geyer. 'Introduction to markov chain monte carlo'. In: *Handbook of markov chain monte carlo* (2011).

[17] W. K. Hastings. 'Monte Carlo sampling methods using Markov chains and their applications'. In: *Biometrika* 57.1 (Apr. 1970), pp. 97–109. DOI: 10.1093/biomet/57.1.97. URL: https://doi.org/10.1093/biomet/57.1.97.

[18] Siddhartha Chib and Edward Greenberg. 'Understanding the Metropolis-Hastings Algorithm'. In: *The American Statistician* 49.4 (Nov. 1995), p. 327. DOI: 10.2307/2684568. URL: https://doi.org/10.2307/2684568.